



1 Intercomparison study and optical asphericity measurements 2 of small ice particles in the CERN CLOUD experiment

3 Leonid Nichman¹, Emma Järvinen², James Dorsey^{1, 3}, Paul Connolly¹, Jonathan Duplissy⁴,
4 Claudia Fuchs⁵, Karoliina Ignatius⁶, Kamalika Sengupta⁷, Frank Stratmann⁶, Ottmar Möhler²,
5 Martin Schnaiter² and Martin Gallagher¹

6 [1]{School of Earth, Atmospheric and Environmental Sciences, University of Manchester, Manchester M13
7 9PL, UK}

8 [2]{Institute of Meteorology and Climate Research, Karlsruhe Institute of Technology, Postfach 3640, 76021,
9 Germany}

10 [3]{National Centre for Atmospheric Science, Manchester, UK}

11 [4]{Department of Physics, P.O. Box 64, 00014 University of Helsinki, Helsinki, Finland}

12 [5]{Laboratory of Atmospheric Chemistry, Paul Scherrer Institute, Villigen, Switzerland}

13 [6]{Leibniz Institute for Tropospheric Research (TROPOS), 04318 Leipzig, Germany}

14 [7]{University of Leeds, School of Earth and Environment, LS2-9JT Leeds, UK}

15

16 *Correspondence to:* Leonid Nichman (Leonid.Nichman@manchester.ac.uk)

17 **Abstract.** Optical probes are frequently used for the detection of microphysical cloud particle properties such as
18 liquid and ice phase, size and morphology. These properties can eventually influence the angular light scattering
19 properties of cirrus clouds as well as the growth and accretion mechanisms of single cloud particles. In this
20 study we compare four commonly used optical probes to examine their response to small cloud particles of
21 different phase and asphericity. Cloud simulation experiments were conducted at the Cosmics-Leaving-
22 Outdoor-Droplets (CLOUD) chamber at European Organisation for Nuclear Research (CERN). The chamber
23 was operated in a series of multi-step adiabatic expansions to produce growth and sublimation of ice particles at
24 super- and sub-saturated ice conditions and for initial temperatures of -30 , -40 and -50 °C. The experiments
25 were performed for ice cloud formation via homogeneous ice nucleation. We report the microphysical properties
26 of small quasi-spherical ice particles in deep convection simulations and small hexagonal ice particles typical
27 for in situ cirrus. Ice crystal asphericity and a degree of submicron complexity deduced from measurements of
28 spatially resolved single particle light scattering patterns by the Particle Phase Discriminator mark 2 (PPD-2K,
29 Karlsruhe edition) were compared with Cloud and Aerosol Spectrometer with Polarisation (CASPOL)
30 measurements and images captured by the 3View Cloud Particle Imager (3V-CPI). Averaged path light
31 scattering properties of the simulated ice clouds were measured using the Scattering-Intensity-Measurements-
32 for-the-Optical-detection-of-ice (SIMONE) and single particle scattering properties were measured by the
33 CASPOL.

34 We show the ambiguity of several optical measurements in ice fraction determination of homogeneously frozen
35 ice, in the case where sublimating quasi-spherical ice particles are present. Moreover, most of the instruments
36 have shown a rather low sensitivity to the crystal complexity for small ice cloud particles that were grown under
37 typical atmospheric conditions. Bulk averaged path depolarisation measurements of these clouds showed higher
38 correlation to single particle measurements at high concentration and small diameters of cloud particles. These
39 results have implications for the interpretation of atmospheric measurements and parametrisations for



1 modelling, particularly for low particle number concentration clouds. This ensemble of optical instruments,
2 using both averaged path and single particle detection presented here, in conjugation with the CLOUD chamber,
3 reveals the possible discrepancies in comparisons of airborne and remote sensing measurements.

4 **1 Introduction**

5 One of the first attempts to distinguish ice particles from water drops in the atmosphere was made almost 70
6 years ago in the Thunderstorm project (Byers and Braham, 1948) during which it was noted that ice particles
7 produce different sound than water drops when they impact the canopy of the aircraft. Since then, there have
8 been many developments of airborne instruments for the measurement of cloud microphysical properties.
9 Wendisch and Brenguier (2013) compiled a comprehensive list covering 48 different instruments, many of
10 which are historical, but recently there have been several new developments, e.g. Abdelmonem et al. (2016) and
11 Baumgardner et al. (2014). Many of the current techniques however are technological improvements on
12 previous instruments originally developed and flown in the 1970's. An ongoing problem is the in situ
13 measurement of concentrations of small ice crystals $< 100 \mu\text{m}$ in size. Accurate measurements of ice crystal size
14 distributions are necessary for evaluation of ice cloud radiative effects, development and evaluation of remote-
15 sensing algorithms, evaluation of aerosol impacts, and ultimately correct representation of ice clouds in climate
16 models (Jensen et al., 2009).

17 This microphysical information is also important in research of early ice formation when initial ice particles in
18 low concentrations push the sampling volume limits of many instruments (Johnson et al. 2014). Optical methods
19 are preferably employed both for remote sensing of clouds and for in situ single particle measurements. For the
20 detection of particle shape and structure, the scattering intensity of single particles is most commonly used. This
21 technique is compared here with the mean scattering intensity from ensemble measurements, where shape
22 information is averaged due to different orientations of the particles in the measuring volume (Sachweh et al.
23 1999).

24 The initial shape of ice particles may be indistinguishable from water droplets. Optically ambiguous shapes of
25 liquid and solid cloud particles such as water, frozen droplets and quasi-spherical ice (Gayet et al., 2012;
26 Järvinen et al., 2016c) may be detected simultaneously in the troposphere. Some of these particle phases coexist
27 for long periods of time e.g. in long-lived mixed-phase stratiform layers (Korolev and Isaac, 2003a). The
28 resolution of most optical probes, coupled with coincidence problems, prevents a clear determination of particle
29 shape for particle sizes smaller than $100 \mu\text{m}$ in such clouds. In glaciated clouds, Cober et al., (2001) applied
30 geometric formulas to 2D images, identifying between 5 and 40 % of them as circular. Spherical particles were
31 observed in large numbers by Korolev and Isaac (2003b) even in clouds sub-saturated with respect to water.
32 Moreover, Lawson et al., (2006) reported that particles $< 50 \mu\text{m}$ account for 99 % of the total number
33 concentration, 69 % of the shortwave extinction, and 40 % of the mass in mid-latitude cirrus. As a result of this
34 shape ambiguity and low resolution of small sizes, our fundamental knowledge of small cloud particle
35 microphysics is far from being complete.

36 Large super-cooled water droplets up to 5 mm in diameter exist only at warmer ambient temperatures, but
37 smaller cloud droplets may frequently exist in a super-cooled state down to $-20 \text{ }^\circ\text{C}$, and less frequently as low as
38 the homogeneous freezing level (Elliott and Smith, 2015; Rosenfeld and Woodley, 2000). Furthermore, very



1 small super-cooled water droplets may stay in a metastable liquid condition down to -40 °C (Korolev et al.,
2 2003a). Pilots often reported deviating around convective clouds due to the danger of ice accretion of super-
3 cooled droplets (Jeanne et al., 2006). Therefore, an inaccurate classification of spherical shapes may directly
4 affect the routes and costs of commercial flights (Gallagher et al., 2016).

5 Frozen droplets are an important feature of mid latitude anvil cirrus. In fact, frozen droplets and frozen droplet
6 agglomerates are a dominant particle type also in higher anvil outflow clouds (Stith et al., 2014; Järvinen et al.,
7 2016c). Frozen droplets could also be responsible for first ice initiation in deep convective clouds (Taylor et al.,
8 2016). Although frozen droplets are frequently measured, our understanding of the microphysical and optical
9 properties of these quasi-spherical ice particles is somewhat vague. The process by which frozen droplets are
10 formed can play an important role in their morphology. Microscopic structures, like surface roughness, as well
11 as detailed information on the aspect ratios of the frozen droplets found in clouds are key variables required to
12 determine the optical parameters that are included in the modelling and prediction of the climate effect of these
13 cloud systems.

14 In addition, quasi-spherical ice shapes are common in cirrus. Luebke et al. (2015), Garrett et al., (2005) report
15 the presence of many quasi-spherical ice particles in cirrus, especially at the smaller sizes. Quasi-spherical ice
16 prevails also in contrails at low temperatures below about -55 °C. In the core of the contrail, high crystal
17 concentrations reduce the vapour density to saturation causing the ice particle to retain a nearly spherical shape
18 (Lawson et al., 1998; Lynch, 2001). Contrail cirrus cover is small compared to natural cirrus; nonetheless, they
19 still have a climatic importance with the constant increase in jet aircraft traffic (Stordal et al., 2005; Irvine and
20 Shine, 2015).

21 Cloud particles measurements on aircraft campaigns inherently suffer from limited spatial coverage and limited
22 instrument sampling volumes. Cirrus clouds do not have an obvious formation stage, and therefore it is not
23 possible to reliably position a research aircraft in their development stage (Lawson et al., 2006). Remote sensing
24 provides averaged features but is insensitive in case of subvisual or contrail cirrus. Conversely, chamber
25 experiments provide a well-controlled and pristine environment for simulations and instrumental comparison,
26 although the role of the ice nucleation process in the atmosphere may change with time through the life cycle of
27 a convective cloud for example, and is strongly influenced by the environmental airflow (Heymsfield et al.,
28 2005).

29 Our chamber campaign investigating the homogeneous freezing process relevant to the upper region of deep
30 convective clouds and in situ formed cirrus in pristine environments was conducted at the European
31 Organisation for Nuclear Research (CERN) in 2013, hereafter referred to as CLOUD 8. The goal of the
32 experiments presented here was to complement and extend the results previously obtained in the Aerosol
33 Interaction and Dynamics in the Atmosphere (AIDA) chamber with similar instruments (Järvinen et al., 2016c;
34 Schnaiter et al., 2016) such as observation of morphological features and confirmation of a possible pathway for
35 quasi-spherical ice formation which affects growth and sedimentation mechanisms of ice in clouds.
36 Additionally, a comparative analysis of four optical probes is reported in this paper to provide clarification of
37 optical measurements in several respects: single particle versus averaged path optical measurements,
38 polarisation measurements versus depolarisation and asphericity derivation i.e. using scattering patterns of the
39 near-forward scattered light in the Particle Phase Discriminator mark 2 (PPD-2K, Karlsruhe edition), single
40 particle polarisation properties in the Cloud and Aerosol Spectrometer with Polarisation (CASPOL), and image



1 analysis in the 3View Cloud Particle Imager (3V-CPI). We then use the asphericity to determine the ice fraction
2 in a cloud by prescribing an aspherical shape for all the ice particles, and hence assume that ice fraction is
3 equivalent to an aspherical fraction.

4 2 Methodology

5 2.1 The CLOUD chamber

6 The chamber facility at CERN is described in detail by Duplissy et al. (2016), Kirkby et al., (2011) and Guida et
7 al., (2013). The expansion system installed at the Cosmics Leaving OUtdoor Droplets (CLOUD) chamber
8 allows production of relatively high cooling rates, above $5\text{ }^{\circ}\text{C min}^{-1}$, compared to the AIDA chamber, where
9 maximum cooling rate of $4\text{ }^{\circ}\text{C min}^{-1}$ is typically achieved (Möhler et al. 2006; Järvinen et al., 2016c). Stronger
10 cooling rates will activate a higher fraction of the aerosol by driving higher peak super-saturation. Since the
11 liquid water content that freezes does not vary with updraft strength, the freezing of more numerous droplets in
12 the faster updrafts simply produces smaller ice particles. This is clearly shown by Ackerman et al. (2015) where
13 ice particle mass distributions in homogeneous freezing for stronger updrafts produce substantially smaller ice
14 particles and greater ice water content. Schnaiter et al. (2016) further showed that high ice particle growth rates
15 also enhance the formation of small-scale complexity, such as ice particle surface roughness. Following the
16 procedure suggested by Schnaiter et al. (2016), we have simulated similar conditions for the derivation of
17 aspherical fractions and instrumental inter-comparison in the CLOUD chamber, where ice particles are
18 sequentially sublimated and then grown under different supersaturated conditions. The multistep adiabatic
19 expansion mechanism has allowed the regrowth of ice after sublimation as will be explained in the next section.

20 2.2 Overview of the homogeneous freezing experiments

21 In the cloud chamber experiments, we have simulated some of the homogeneous freezing processes taking place
22 in the deep convective cloud systems i.e. with updraft velocities up to 5 m s^{-1} with corresponding cooling rates
23 up to $5.8\text{ }^{\circ}\text{C min}^{-1}$. In the following sections we present the evolution of the ice particle shape and small-scale
24 complexity upon freezing, sublimation and re-growth periods from selected representative individual
25 experimental runs. Overall, all the results from repeated individual experiments agreed well with each other. A
26 representative list of the conducted experiments can be found in Table 1. The technical description of the
27 CLOUD chamber pressurisation, CCN injection and expansion of the air volume in a multi-step regime is given
28 in detail elsewhere (Nichman et al., 2016; Duplissy et. al., 2016; Guida et al., 2012, 2013) and will be briefly
29 described here.

30 The homogeneous freezing experiments were started in a pressurized chamber volume, at 123.3 kPa, with a
31 CCN injection. The sulphuric acid solution droplets, used as CCN, were generated in a sulphuric acid generator
32 consisting of heated sulphuric acid reservoir and airflow past the reservoir. A more detailed explanation of the
33 generation method can be found in Wagner et al. (2008). By varying the duration of the sulphuric acid injection,
34 we controlled the number concentration of the sulphuric acid droplets, and by adjusting the temperature of the
35 sulphuric acid reservoir and the airflow rate through the heated reservoir we controlled the mean size of the
36 aerosol particles.



1 The chamber is surrounded by an insulated thermal housing which allows a precise regulation of the
2 temperature with stability within 0.1 °C. The in situ temperature values are measured close to the centre of the
3 chamber, at 1.2 m distance from the walls using a PT100 temperature sensor (Duplissy et al., 2016; Dias et al.,
4 2016). For pressure monitoring in the chamber, we used the VEGABAR 53 process pressure transmitter,
5 VEGA.

6 At the beginning of most experiments, we generated low concentrations ($\sim 100 \text{ cm}^{-3}$) of sulphuric acid aerosol.
7 At these concentrations, all seed aerosols will act as CCN at almost the same time and further homogeneous
8 nucleation and growth of the ice crystals would occur upon further expansion cooling. All the experiments were
9 initiated slightly below ice saturated conditions at temperatures near -30 , -40 and -50 °C. In the experiments
10 starting at -30 °C we cooled the chamber air by expanding the volume until super cooled liquid droplets were
11 formed. The droplets were grown by further cooling until ice started to form by homogeneous freezing of the
12 super-cooled water droplets. The ice particles then grew until the expansion was stopped and the formed ice
13 crystals started to sublime under ice sub-saturated conditions, induced by an increase of temperature due to the
14 heat flow from the warm chamber walls. A second step in the expansion profile allowed the regrowth of the
15 sublimating particles. The experiments at -40 and -50 °C were started similarly by cooling the chamber volume
16 until the first ice particles were formed by deposition nucleation. After the first ice particles were detected and
17 had grown in diameter (Table 1), we proceeded to the next step of the multistep expansion profile as discussed
18 above.

19 **2.3 Cloud probes**

20 **2.3.1 PPD-2K**

21 The classification of cloud particles by the PPD-2K is based on a spatial analysis of high resolution intensity
22 patterns of single particles in the 5 to 26° forward angular range. In the scattering patterns of (spherical) droplets
23 we normally observe concentric rings at angular positions corresponding to the maxima intensities given by
24 Mie-theory. We used computerised discrimination of images with concentric rings from images without the
25 rings based on variance calculation of the image pixels along the polar integrated azimuthal intensity profiles
26 (Vochezer et al., 2016). Aspherical fractions were determined by applying a threshold variance value of 10^{-5} .
27 Images with low variance corresponded to concentric rings and were classified as spherical (e.g. droplets).
28 Similarly, in the case of ice particles with mean variance below this value the particles were classified as
29 spherical. Ice habits e.g. columns and plates have characteristic scattering patterns which allow classification of
30 the detected particles. More technical details are described in Vochezer et al. (2016).

31 **2.3.2 SIMONE**

32 The averaged path SIMONE-Junior (Järvinen et al., 2016b), was installed in the chamber for bulk depolarisation
33 measurements. This instrument is comparable to a lidar and is used to detect phase-transitions in aerosol, cloud
34 particle ensembles, and to investigate the microphysical properties of clouds. The instrument projects a 552 nm
35 polarised (e.g. perpendicular, parallel and circular) light beam and detects from a volume of a few cubic
36 centimetres. Unlike a lidar measurement, parallel and perpendicular components of the backscattered light are
37 measured around the detection angle of 176° , at a very confined angular range with an acceptance angle less
38 than 0.8 mrad. The linear depolarisation ratio is zero for spherical particles and non-zero if particles' shape



1 deviates from a sphere, thus a detection of the bulk cloud phase is possible. Forward scattering intensity is
2 measured at 4° . The operation of the SIMONE in the CLOUD chamber is described in detail by Järvinen et al.
3 (2016a). The basic instrument concept and data interpretation in case of chamber ice clouds is detailed in
4 Schnaiter et al. (2012).

5 **2.3.3 Airborne probes**

6 **CASPOL**

7 The CASPOL installed in the chamber was part of the Cloud, Aerosol, and Precipitation Spectrometer (CAPS,
8 Droplet Measurement Technologies), an instrument commonly used on aircraft for cloud microphysical
9 measurements (e.g. Baumgardner et al., 2001; Johnson et al., 2012; Luebke et al., 2015). The CASPOL relies on
10 incident laser-scattering by single particles. The collecting optics guide the light scattered in the 4 to 12°
11 subtended cone into a forward-sizing photodetector. This light is measured and used to infer particle size.
12 However, the CASPOL is calibrated with spheres and aspherical particles are mis-sized (Borrmann et al., 2000).
13 We estimate the sizing error would normally be of the order of the size bin width.
14 The backscatter detector measures the scattered light cone subtended by the angles 168 to 176° . Additionally,
15 this version of CASPOL measures the polarised fraction of the backscattered light in the orthogonal plane for
16 the first 292 particles s^{-1} (Droplet Measurement Technologies Manual, 2011). This functionality allows
17 discrimination of aspherical particles in the $0.51 - 50 \mu\text{m}$ range. For spherical particles, typically droplets, the
18 polarisation of the incident light will be preserved and the orthogonal polarisation in the back-scatter will
19 generate nearly zero signal. Depending on the asphericity of the particles, there will be increased signal in the
20 backscatter polarised detector. An increase in size with decrease in polarisation in CASPOL at temperatures
21 below the frost point will mean that ice is sublimating and becoming more spherical (Jensen et al., 2010). The
22 classification of droplets and ice in CASPOL data analysis is primarily based on polarisation threshold which
23 needs to be determined from laboratory experiments (Nichman et al., 2016).

24 **3VCPI**

25 Another aircraft mounted instrument is the Cloud Particle Imager which can image and count particles in the
26 size range of $15\text{--}2500 \mu\text{m}$, with the images having a nominal $2.3 \mu\text{m}$ resolution. The newer 3V-CPI (SPEC Inc.)
27 is essentially a 400 frame per second CPI probe integrated with a 2D-S probe. CPI obtained information covers
28 particle size (including area and volume) and ice habit classification (Heymsfield et al., 2010). Complementary
29 size distributions and concentrations data are obtained by the 2D-S. The 3V-CPI is especially suitable for use in
30 ice and mixed phase clouds (Lawson et al., 2003; Gayet et al., 2012; Stith et al., 2014). Each of the $2.3 \mu\text{m}$
31 resolved surface images captured by the CPI can be fitted to a circle function to determine the roundness of the
32 particle (Korolev and Isaac, 2003b). Temporal changes of roundness can be used to calculate the mean non-
33 round (aspherical) concentration fraction. However, the roundness parameter for smallest detected particles of
34 $10 \mu\text{m}$ optical diameter, have the largest uncertainty as will be discussed in Sect. 3.2.



1 3 Results and discussion

2 3.1 Experimental description

3 3.1.1 Ice nucleation and regrowth

4 The air pressure and mean temperature profiles for a typical expansion procedure in accordance with Schnaiter
5 et al. (2016) are presented in Fig. 1a. The expansion starts first with a slow pressure decrease to create water-
6 supersaturated conditions inside the chamber and to form a cloud of super-cooled droplets. The expansion rate is
7 increased towards the end in order to achieve ice-supersaturated conditions in a short time period and to nucleate
8 the ice almost simultaneously. The overall cooling rate during this expansion was -4.9 °C min^{-1} . The PPD-2K
9 measured the size distribution during the expansion (Fig. 1b). The cloud period with super-cooled droplets lasts
10 only a few seconds and followed by almost immediate and fast ice formation. The depolarisation signal
11 measured by the SIMONE increases promptly after the increase in the forward scattering signal indicating the
12 short droplet period followed by the fast formation of ice (Fig 1c). The expansion is then stopped at ~ 1 min
13 (Fig. 1a).

14 After the first step of the expansion, the initial temperature of the air volume is slowly restored by the heat flux
15 from the warmer chamber walls, thus creating sub-saturated conditions inside the chamber. This warming leads
16 to the sublimation of ice crystals and the observed changes in their microphysical properties. A re-growth of the
17 sublimating ice crystals is initiated at ~ 11 min, when the pressure decreases from 111.3 to 101.8 kPa. The
18 depolarisation signal increases once again during this step and reaches slightly higher levels (0.34) than in the
19 first step (0.26), together with an increasing noise level due to the low number concentration. There is also a
20 small increase in the forward scattering but this is much lower than in the first step of the expansion due to ~ 5
21 fold decrease in the concentration. We assume a complete glaciation in the first step without any significant
22 reactivation in the number concentration during the regrowth period (Fig 1c).

23 3.1.2 Size range overlap

24 In this comparison, the overlapping size range of PPD-2K and CASPOL for measurements of small ice particles
25 is $7 - 50\text{ }\mu\text{m}$ (Fig. 1b). However, only 41 % of the particle-by-particle (PBP) polarisation data in CASPOL at $-$
26 30 °C were from particles larger than $7\text{ }\mu\text{m}$. At lower temperatures the particle size distribution (PSD) is shifted
27 towards the grey area in Fig. 2, below the PPD-2K size cut-off. The fraction of CASPOL PBP polarisation data
28 points from particles $> 7\text{ }\mu\text{m}$ at lower temperatures was even lower: 24 % (-40 °C), 32 % (-50 °C), thus, most
29 of the particles in the cloud that produce the polarisation data in the CASPOL are small, $< 7\text{ }\mu\text{m}$, while in the
30 PPD-2K data 100% of the analysed particles are $> 7\text{ }\mu\text{m}$.

31 The size segregated aspherical fractions as measured by the PPD-2K in the overlapped size region are presented
32 in Fig. 3. At -30 °C , the large ice particles reach $20\text{ }\mu\text{m}$ in diameter during the first step of the expansion and
33 grow up to $35\text{ }\mu\text{m}$ during the second step, within the detection range of CASPOL. Ice particles formed under
34 different temperature regimes would have a different morphology. At cirrus temperatures below -40 °C , the ice
35 particles form directly from the vapour phase via deposition nucleation (Figs. 3b, 3c), a different formation
36 pathway compared to ice formation through the liquid phase at -30 °C (Fig. 3a). At the final step of the
37 expansion at -30 °C , during the sublimation period, the aspherical fraction is extremely low due to sphericity
38 ambiguity as will be discussed in Sect. 3.3. For better statistical characterisation we achieved longer cloud life



1 time at lower temperatures, up to 45 min. However the measurements of PPD-2K at these temperatures were
2 somewhat incomplete, missing the smaller sizes and hence the initial steps of cloud particle formation and
3 growth especially during the first step of the expansion (Figs. 3b, 3c). The temperatures profiles of runs:
4 1276.05 (−40 °C), and 1298.12 (−50 °C) are shown in Fig. S1.

5 3.1.3 Column fraction

6 The ice fraction contains ice habits such as plates and columns in all the regrowth experiments discussed here
7 (Table 1). The largest fraction detected by PPD-2K at different temperatures was composed of ice columns as
8 shown in Fig. 4. In the first part of experiment 1292.01 (−30 °C) the frozen droplets are grown at lower
9 temperature and higher super-saturation than in the second sublimation period of this experiment (Fig. 1a),
10 leading to a formation of complex particles (Sect. 3.3). In the regrowth period, the temperature drop and super-
11 saturation conditions are more moderate and we observe the formation of columnar ice particles. The columnar
12 shape is not preserved and the ice particles sublimate to their underlying spherical core as seen in Fig. 3a. The
13 largest column fractions were measured at the lowest temperature −50 °C (Fig. 4c). Although we know that
14 diffraction instruments (e.g. SID-1, SID-2, SID-3, Hirst et al., 2001; Cotton et al., 2010; Vochezer et al., 2016)
15 suffer from major coincidence errors at high concentration and mixed phase clouds, in these chamber
16 experiments we did not observe coincidence errors.

17 3.2 3V-CPI image analysis of ice particles

18 High concentrations of particles grew above 20 μm in diameter (Fig. 1b), thus allowing their detection with the
19 3V-CPI instrument. Quasi-spherical or quasi-spheroidal small particles were identified from the CPI images
20 (Fig. 5). The CPI imager is triggered by the 2D-S component for particles larger or equal to 10 μm as described
21 in Sect. 2.3.3. The image analysis can provide the roundness of the particles. Due to the larger error in small
22 sizes, Korolev and Isaac (2003b) have considered the roundness of the particles with diameter larger than 20 μm
23 is appropriate. Connolly et al. (2007) have included the roundness of smaller particles of 10 μm in diameter in
24 their analysis using size and shape corrections based on tests with ice analogues to the instrument's depth of
25 field. Emersic et al. (2015) chose a roundness threshold of 0.9 for phase discrimination of particles larger than
26 35 μm. The exact definition and calculations of roundness are described in detail in the papers above. In this
27 analysis we consider particles in the range of 20–50 μm for broader coverage of the CASPOL and PPD-2K size
28 ranges while constraining the uncertainty in the roundness parameter. Here, the threshold for phase
29 discrimination by roundness was set to 0.9.

30 Analysis of a large dataset of CPI images by Korolev et al., (2003c) showed that in glaciated clouds a large
31 fraction of particles with diameter < 60 μm do indeed have a quasi-spherical compact shape. Korolev and Isaac,
32 (2003b) noted that the question of spherical ambiguity remains due to optical limitations of the instruments.
33 Despite the limitations of size range and resolution, Fig. 6a shows an increase of the non-round image fraction
34 during the growth periods of the ice particles in our chamber experiments.

35 3.3 Aspherical fractions measured by PPD-2K, CASPOL, 3V-CPI

36 In airborne measurements, ice fractions are commonly derived from the optical asphericity of the particles (Sect.
37 1). Here we compare PPD-2K and CASPOL single particle measurements to examine their ability to distinguish



1 between droplets and ice particles in different ice nucleation modes. In experiment no. 1292.01 ($-30\text{ }^{\circ}\text{C}$), all the
2 droplets freeze simultaneously, almost immediately after their formation, concluding the duration of the pure
3 liquid cloud in the order of seconds (Fig. 6a). Promptly after freezing we measure a high ice (aspherical)
4 fraction ($\sim 100\%$), as expected. The freezing onset is detected by the increase in the depolarisation signal from
5 the SIMONE, and proceeds with an increase in 3V-CPI non-round fraction (Sect. 3.2), both indicating the
6 presence of non-spherical particles. In the sublimation period, at 4 min, we see the reversed transition in the
7 aspherical fraction; we start to detect more spherical particles that are classified as liquid droplets according to
8 the thresholds used to classify ice (Sect. 2.3; Nichman et al., (2016)). The depolarisation finally decreases (Fig.
9 6a), and particles are no longer detected by the 3V-CPI due to their decrease in size below the threshold. The
10 size segregated ice fraction for this experiment is shown in Fig. 3a.

11 During the sublimation periods the aspherical fraction decreases implying increasing sphericity of the particles
12 (Fig. 6a). However, once full glaciation was observed, the liquid phase cannot subsequently exist at the ambient
13 chamber temperature; below $-30\text{ }^{\circ}\text{C}$. Therefore, the nearly spherical particles observed (4–10 min, 19 min) are
14 spherical ice and not liquid water droplets. In atmospheric measurements, such an aspherical fraction would
15 normally be converted into an ice fraction. In this cloud simulation, at the end of the sublimation period, both
16 instruments misinterpret the total ice fraction as spherical-liquid by 60%.

17 In experiments 1276.05 ($-40\text{ }^{\circ}\text{C}$) and 1298.12 ($-50\text{ }^{\circ}\text{C}$) (Figs. 5b, 5c), we observe a lower aspherical fraction
18 measured by the CASPOL at a lower temperature. Polarisation data analysis therefore suggests that ice particles
19 smaller than $7\text{ }\mu\text{m}$ are more spherical at lower temperatures (Fig. 6c red line) and they are more abundant (Sect.
20 3.1.2). Furthermore, the aspherical fraction for all particles detected in the PBP mode in CASPOL at $-50\text{ }^{\circ}\text{C}$
21 follows the SIMONE depolarisation time series while the aspherical fraction of CASPOL $>7\text{ }\mu\text{m}$ subgroup is
22 higher and increases towards the end of the expansion (Fig. 6c). The size dependence of these two polarisation
23 detection techniques is demonstrated in Sect. 3.4. However, scattering patterns detected by the PPD-2K showed
24 a 100% aspherical fraction in both experiments with vapour formed ice crystals.

25 Similar discrepancies in aspherical fraction measurements by PPD-2K and CASPOL were shown already by
26 Järvinen et al., (2016c) for ice particles formed via homogeneous nucleation and via deposition nucleation on
27 mineral dust at $-30\text{ }^{\circ}\text{C}$. The asphericity of the particles significantly differs for ice formed through the liquid
28 phase and ice formed through the vapour phase. These discrepancies (Figs. 5b, 5c) at lower temperatures can be
29 partially explained by the decrease in the number of particles measured in every second and therefore large
30 standard deviation in aspherical fraction calculation i.e. 19 % for particles $>7\text{ }\mu\text{m}$ at $-40\text{ }^{\circ}\text{C}$ and 37 % for
31 particles $>7\text{ }\mu\text{m}$ at $-50\text{ }^{\circ}\text{C}$. However, the smaller size of particles at $-40, -50\text{ }^{\circ}\text{C}$ is the main cause to reduced
32 sensitivity of the polarisation measurements in respect to aspherical features as will be explained in the next
33 subsection.

34 **The impact of small-scale surface complexity on phase discrimination**

35 The resolution of instrumentation employed in atmospheric measurements, commonly, is not sensitive enough
36 to image the surface microstructural features of the ice crystals. The resolution of the widely used CPI probe is
37 around $2\text{ }\mu\text{m}$, i.e. in the same range as the smallest droplets that are frozen into ice crystals and significantly
38 larger than the size of the ice crystals' surface anomalies. Although these anomalies, like roughness and stepped



1 hollowness of the crystal, do not significantly contribute to the mass distribution, they can significantly alter the
2 light scattering properties of the ice crystals, as discussed in the introduction.
3 We have analysed the scattering patterns of the PPD-2K instrument to determine the surface features of
4 individual ice crystals as described in detail in Schnaiter et al. (2016). This instrument is sensitive to features
5 that are on the order of the wavelength used, 532 nm. The particle's surface complexity or non-uniformity
6 manifests itself as speckles in the diffraction patterns (Järvinen et al., 2016c), where the analysis of spatial
7 uniformity of the scattered light intensity with the Grey-level Co-Occurrence Matrix (Schnaiter et al., 2016)
8 indicates the small-scale complexity of an ice crystal. The so called k-value defined as a complexity parameter
9 by Schnaiter et al. (2016) can reflect the physical complexity in a higher k-value. However we should emphasize
10 that at present it is not possible to quantitatively relate this value to an actual degree of complexity or surface
11 uniformity of the particle. We also note here that although a k-value can be calculated from the PPD-2K
12 instrument, the k-value is not calibrated for this instrument. Therefore, in this study we can only conclude about
13 the relative variations in this complexity parameter.

14 Figure 7a shows the size segregated k-value in experiment no. 1292.01. The experiment starts with a period of
15 super cooled liquid droplets, where scattering patterns of concentric rings are observed (scattering pattern A in
16 Fig. 7a). The freezing of the droplets takes place almost simultaneously and all the freshly frozen droplets
17 exhibit surface features i.e. the PPD-2K scattering patterns are speckled without the normal concentric ring
18 features (scattering pattern B in Fig. 7a). Seemingly the frozen droplets develop a frost layer (Järvinen 2016c)
19 on their surfaces during the freezing and initial growth. However this layer was too thin to be detected by the
20 other instruments.

21 During the sublimation period, the complexity of particles noticeably decreased (Fig. 7b). The smooth frozen
22 droplets were found at smaller sizes compared to the frozen droplets with small-scale complexity. The
23 sublimation of the frost can be seen in scattering patterns C and D (Fig. 7), where the diffraction pattern D
24 cannot easily be distinguished anymore from that of a liquid droplet, i.e. the frozen droplet in question is almost
25 a perfect sphere.

26 The re-growth of the sublimating frozen droplets, achieved by again starting expansion leading to ice super
27 saturated conditions. The surface frost layer developed again immediately after super saturation is reached and
28 the median complexity parameter reaches its' highest value (Fig. 7b). Consequently, these particles are
29 immediately classified as aspherical. The observed complexity of pattern B reappears on pattern E i.e. on the
30 columns (Figs. 4a, 7). The re-grown ice crystals were again allowed to sublimate after the growth period.
31 Similar smooth frozen droplets were detected as in the first sublimation period, together with a decline of the
32 detected aspherical fraction.

33 The small-scale complexity significantly changes the scattering patterns measured by the PPD-2K (Fig. 7).
34 Therefore, the observed speckled patterns can be easily classified as aspherical, which leads to a robust and high
35 ice fraction, if complex ice particles are present. Sublimating columnar particles that demonstrate lower
36 complexity (Fig. S2) are classified as aspherical in the PPD-2K. Only optically spherical sublimating frozen
37 droplets are misclassified as droplets by the automatic algorithm. However, with visual inspection it is still
38 possible to discriminate between a smooth ice sphere and a spherical liquid droplet (compare patterns A and D
39 in Fig. 7). However, other optical instruments (e.g. CASPOL) can misclassify complex ice particles if they are
40 too small, and underestimate the aspherical fraction if their occurrence is low.



1 3.4 Single particle polarisation and ensemble depolarisation ratios

2 This analysis aimed at improving our interpretation of the small ice particle polarizability and the comparison of
3 different instruments and their approaches to discriminate small liquid and ice phase cloud particles by
4 properties of the scattered light. One such property is the linear depolarisation ratio for parallel incident laser
5 polarisation $\delta_{||}$ which is defined as the perpendicularly polarised to parallel polarised ratio of the backscattered
6 light intensity ($I_{\perp}/I_{||}$). This ratio is frequently used in remote sensing (e.g. Burton et al., 2012; Petzold et al.,
7 2010). The linear polarisation ratio in CASPOL data analysis is defined as the fraction of the perpendicularly
8 polarised backscattered light from the total backscattered intensity ($D_{pol}/Back$) as previously reported (Glen
9 and Brooks, 2013) and is used for ice fraction derivation (Nichman et al., 2016). The particle detection method
10 and the measured polarisation components are not the only dissimilarities in these instruments, they also operate
11 at different wavelengths, have slightly different collection angles and two orders of magnitude difference in the
12 sample volume (see Sect. 2.3).

13 Depolarisation ratio measured by the SIMONE and the polarisation ratio measured by the CASPOL were
14 plotted against each other with 1 s temporal resolution for run no. 1292.01 (high concentration and small
15 diameter), no. 1291.12 (low concentrations and big diameter), no. 1291.07 (high concentration and small
16 diameter) and no. 1298.2 (low concentration and small diameter) (Table 1) are shown in Fig. 8. The dimensions
17 of the marker reflect the number concentration, with the highest at 56 cm^{-3} . The CASPOL polarisation ratios
18 presented here are based on 1 s averages for all particles larger than $3 \mu\text{m}$. Small aerosol particles ($< 3 \mu\text{m}$) were
19 detected during background measurements; after CCN injection and before the expansion. These small particles
20 i.e. non-activated aerosols were excluded from further analysis.

21 The Lowest correlation was found at low concentration, where the detected polarisation is higher than the
22 depolarisation. This is partially due to the averaging deviation at low concentration within the large sample
23 volume of the SIMONE instrument. Nonetheless, in several cases a surprisingly reasonable correlation is
24 observed (Fig. 8a, 8b). Generally, we have found that higher correlation is observed between the different
25 instruments in cases with high concentration and small diameters of cloud particles ($R^2 \sim 0.35$). Low correlation
26 ($R^2 \sim 0.01$) is observed in cases with low concentrations and larger sizes of cloud particles.

27 3.5 Implications to atmospheric measurements

28 The classification of quasi-spherical ice as liquid droplets is posing a problem in atmospheric measurement and
29 especially in mixed-phase clouds, where the ice fraction calculations can be affected by the misinterpretation
30 presented in this paper. In these chamber experiments, we know that all the particles in the sub-saturated
31 conditions are in the ice phase, which allows us to use the spherical classification method to distinguish
32 spherical ice particles in cold clouds. In the atmosphere, there are additional possible crystal rounding
33 mechanisms e.g. equilibrium thermal roughening near $0 \text{ }^{\circ}\text{C}$, a surface coating of solution, kinetic roughening at
34 high super saturations, and latent heat-induced melting of the surface during growth at high temperatures and
35 super saturation. In addition, frozen droplets retain their rounded appearance until sufficient growth occurs.
36 Therefore, it is not possible to infer sub-saturated conditions in the atmosphere merely by sampling rounded
37 crystals (Nelson 1998) and the measured ice fraction is prone to significant underestimation. In any case of
38 small quasi-spherical particles detection at sub-zero temperatures in the atmosphere, we recommend to compare
39 the data of more than one instrument. Ice fraction derived from CASPOL data can be compared to other



1 instruments with higher confidence when the PSD is fully covered by the overlapped size and concentration
2 range of the instruments with sufficient number of particles for ice fraction derivation and low standard
3 deviation. However, high concentration may cause coincidence and misestimation of the ice fraction.
4 The comparison of remote sensing and PBP measurements is not a straightforward process (i.e. bulk vs. single
5 particle and single complexity vs mixed-complexity ensembles of particles). Many single particle laboratory
6 techniques in particular have proven difficult to adopt when translated to real atmospheric environments. These
7 techniques often provide complementary data rather than comparable data (Lynch, 2001) and research in this
8 area continues. Based on our analysis, ensemble depolarisation measurements of cloud particles at certain
9 concentrations, sizes and atmospheric conditions can be comparable to single particle airborne measurements.

10 4 Conclusions

11 We have presented an instrumental setup for combined single cloud particle and ensemble measurements for
12 assessment of the relative optical ice and liquid responses in each case. The results were used to determine the
13 ice shape and small-scale complexity evolution during adiabatic expansion, sublimation and regrowth as well as
14 for potential impact on phase discrimination. We report observations of super-cooled and frozen droplets, small
15 ice habits and spheroids in a series of CLOUD chamber experiments at -30 , -40 and -50 °C.

16 We have shown that the small quasi-spherical ice particles produced in the sublimation process exhibit a similar
17 optical behaviour to that of water droplets in the PPD-2K variance analysis and in the CASPOL polarisation
18 analysis for high PSD overlap at -30 °C. The analysis of the scattering patterns shows the similarity of the
19 spherical states and the difficulty in applying automatic phase discrimination. Therefore, observations of small
20 spheroids (< 60 μm) in sub-saturated conditions might be highly ambiguous. These results indicate that small
21 quasi-spherical ice misclassification might similarly concern numerous optical instruments, impactors and other
22 probes that were not examined here. Nonetheless, the scattering patterns differ for quasi-spherical ice and water
23 due to small deviations from sphericity. An increase of resolution in future versions of the optical instruments
24 might amplify this discrimination and reveal additional subtle features.

25 We have shown a chamber simulation of small-scale complexity evolution on a frozen droplet during an updraft
26 and in sub-saturated conditions. In regions with high concentration of small cloud particles (< 60 μm), the
27 observed differences in morphology will affect the observed radiative properties, growth mechanisms,
28 aggregation and charging in clouds. The aspherical fraction detected by the PPD-2K could be described with a
29 high degree of small-scale complexity which was undetectable by the other instruments. This complexity
30 measurement can be potentially calibrated in future experiments to derive the complex fraction of ice particles.
31 However, the complexity of ice particles smaller than 7 μm remains unclear.

32 We have presented polarisation measurements of airborne and laboratory-instruments in an expansion chamber.
33 We conclude that in these simulated atmospheric conditions the polarisation and depolarisation signal from
34 frozen droplets have higher correlation at higher concentrations of small particles and can be comparable above
35 certain concentration and size thresholds. These findings and the derived instrumental differences can be used in
36 the interpretation of atmospheric measurements of frozen droplets from remote and in situ, combined campaigns
37 as well as a pathway for further research and development of these instruments.

38



- 1 *Acknowledgments.* We would like to thank CERN for supporting CLOUD with important technical and financial
- 2 resources. We express great appreciation for the CLOUD collaboration. This research has received funding from
- 3 the EC Seventh Framework Programme (Marie Curie Initial Training Network “CLOUD-TRAIN” no. 316662).
- 4 The SIMONE measurements were funded by the CERN CLOUD project. The PPD-2K instrument was fully
- 5 funded by the Deutsche Forschungsgemeinschaft within project SCHN 1140/2-1. The CAPS and 3V-CPI
- 6 instruments used in this work were supplied by the UK National Centre for Atmospheric Science.



1 References

- 2 Abdelmonem, A., Järvinen, E., Duft, D., Hirst, E., Vogt, S., Leisner, T., and Schnaiter, M.: PHIPS-HALO: The
3 airborne Particle Habit Imaging and Polar Scattering probe. Part I: Design and Operation, Atmos. Meas. Tech.
4 Discuss., doi:10.5194/amt-2016-42, in review, 2016.
- 5 Ackerman, A. S., Fridlind, A. M., Grandin, A., Dezitter, F., Weber, M., Strapp, J. W., and Korolev, A. V.: High
6 ice water content at low radar reflectivity near deep convection – Part 2: Evaluation of microphysical pathways
7 in updraft parcel simulations, Atmos. Chem. Phys. Discuss., 15, 16551-16613, doi:10.5194/acpd-15-16551-
8 2015, 2015.
- 9 Baumgardner, D., Jonsson, H., Dawson, W., O'Connor, D., and Newton, R.: The cloud, aerosol and precipitation
10 spectrometer: a new instrument for cloud investigations, Atmospheric Research, 59, 251-264, doi:
11 10.1016/S0169-8095(01)00119-3, 2001.
- 12 Baumgardner, D., Newton, R., Krämer, M., Meyer, J., Beyer, A., Wendisch, M., and Vochezer, P.: The Cloud
13 Particle Spectrometer with Polarization Detection (CPSPD): A next generation open-path cloud probe for
14 distinguishing liquid cloud droplets from ice crystals, Atmospheric Research, 142, 2-14,
15 <http://dx.doi.org/10.1016/j.atmosres.2013.12.010>, 2014.
- 16 Borrmann, S., Luo, B., and Mishchenko, M.: Application of the T-matrix method to the measurement of
17 aspherical (ellipsoidal) particles with forward scattering optical particle counters, J. Aerosol Sci., 31, 789-799,
18 doi:10.1016/S0021-8502(99)00563-7, 2000.
- 19 Burton, S. P., Ferrare, R. A., Hostetler, C. A., Hair, J. W., Rogers, R. R., Obland, M. D., Butler, C. F., Cook, A.
20 L., Harper, D. B., and Froyd, K. D.: Aerosol classification using airborne High Spectral Resolution Lidar
21 measurements – methodology and examples, Atmos. Meas. Tech., 5, 73-98, doi: 10.5194/amt-5-73-2012, 2012.
- 22 Byers, H. R., and Braham, R. R.: Thunderstorm structure and circulation, J. Meteor., 5, 71-86, doi:
23 10.1175/1520-0469(1948)005<0071:TSAC>2.0.CO;2, 1948.
- 24 Cober, S. G., Isaac, G. A., Korolev, A. V., and Strapp, J. W.: Assessing Cloud-Phase Conditions, Journal of
25 Applied Meteorology, 40, 1967-1983, doi:10.1175/1520-0450(2001)040<1967:ACPC>2.0.CO;2, 2001.
- 26 Connolly, P. J., Flynn, M. J., Ulanowski, Z., Choularton, T. W., Gallagher, M. W., and Bower, K. N.:
27 Calibration of the Cloud Particle Imager Probes Using Calibration Beads and Ice Crystal Analogs: The Depth of
28 Field, Journal of Atmospheric and Oceanic Technology, 24, 1860-1879, doi: 10.1175/JTECH2096.1, 2007.
- 29 Cotton, R., Osborne, S., Ulanowski, Z., Hirst, E., Kaye, P. H., and Greenaway, R. S.: The Ability of the Small
30 Ice Detector (SID-2) to Characterize Cloud Particle and Aerosol Morphologies Obtained during Flights of the
31 FAAM BAe-146 Research Aircraft, Journal of Atmospheric and Oceanic Technology, 27, 290-303, doi:
32 10.1175/2009JTECHA1282.1, 2010.
- 33 Dias, A., Ehrhart, S., Vogel, A., Williamson, C., Simões, J., Kirkby, J., Mathot, S., and Onnela, A.: Analysis of
34 temperature homogeneity of the CLOUD chamber at CERN, in preparation, 2016
- 35 Droplet Measurement Technologies Manual: CAPS operator manual, DOC-0066 Revision F, DMT, Boulder,
36 Colorado, USA, 2011.
- 37 Duplissy, J., Merikanto, J., Franchin, A., Tsagkogeorgas, G., Kangasluoma, J., Wimmer, D., Vuollekoski, H.,
38 Schobesberger, S., Lehtipalo, K., Flagan, R., Brus, D., Donahue, N., Vehkämäki, H., Almeida, J., Amorim, A.,
39 Barmet, P., Bianchi, F., Breitenlechner, M., Dunne, E., Guida, R., Henschel, H., Junninen, H., Kirkby, J.,
40 Kürten, A., Kupc, A., Määttänen, A., Makhmutov, V., Mathot, S., Nieminen, T., Onnela, A., Praplan, A.,



- 1 Riccobono, F., Rondo, L., Steiner, G., Tome, A., Walther, H., Baltensperger, U., Carslaw, K., Dommen, J.,
2 Hansel, A., Petäjä, T., Sipilä, M., Stratmann, F., Vrtala, A., Wagner, P., Worsnop, D., Curtius, J., and
3 Kulmala, M.: Effect of ions on sulfuric acid-water binary particle formation II: Experimental data and
4 comparison with QC-normalized classical nucleation theory, *Journal of Geophysical Research: Atmospheres*,
5 doi:10.1002/2015JD023539, 2016.
- 6 Elliott, J. W., and Smith, F. T.: Ice formation on a smooth or rough cold surface due to the impact of a
7 supercooled water droplet, *Journal of Engineering Mathematics*, 1-30, doi:10.1007/s10665-015-9784-z, 2015.
- 8 Emersic, C., Connolly, P. J., Boulton, S., Campana, M., and Li, Z.: Investigating the discrepancy between wet-
9 suspension- and dry-dispersion-derived ice nucleation efficiency of mineral particles, *Atmos. Chem. Phys.*, 15,
10 11311-11326, doi: 10.5194/acp-15-11311-2015, 2015.
- 11 Gallagher, M.W., Baumgardner, D., Lloyd, G., Beswick, K., Freer, M., and Durant, A.: Detection and Analysis
12 of High Ice Concentration Events and Supercooled Drizzle from IAGOS Commercial Aircraft, *Geophys. Res.*
13 *Abstr.* Vol. 18, EGU2016-2924, EGU General Assembly, Vienna, Austria, 2016.
- 14 Garrett, T. J., Navarro, B. C., Twohy, C. H., Jensen, E. J., Baumgardner, D. G., Bui, P. T., Gerber, H., Herman,
15 R. L., Heymsfield, A. J., Lawson, P., Minnis, P., Nguyen, L., Poellot, M., Pope, S. K., Valero, F. P. J., and
16 Weinstock, E. M.: Evolution of a Florida Cirrus Anvil, *J. Atmos. Sci.*, 62, 2352–2372, 2005.
- 17 Gayet, J. F., Mioche, G., Bugliaro, L., Protat, A., Minikin, A., Wirth, M., Dörnbrack, A., Shcherbakov, V.,
18 Mayer, B., Garnier, A., and Gourbeyre, C.: On the observation of unusual high concentration of small chain-like
19 aggregate ice crystals and large ice water contents near the top of a deep convective cloud during the CIRCLE-2
20 experiment, *Atmos. Chem. Phys.*, 12, 727-744, doi:10.5194/acp-12-727-2012, 2012.
- 21 Glen, A. and Brooks, S. D.: A new method for measuring optical scattering properties of atmospherically
22 relevant dusts using the Cloud and Aerosol Spectrometer with Polarization (CASPOL), *Atmos. Chem. Phys.*,
23 13, 1345–1356, doi:10.5194/acp-13-1345-2013, 2013.
- 24 Guida, R., Carrie, P., De Menezes, L., Duplissy, J., Fayet, F., Kirkby, J., Mathot, S., Minginette, P., Onnela, A.,
25 Rochez, J., Thomas, G., Wasem, A., and Wilhelmsson, M.: An ultra-pure gas system for the CLOUD
26 experiment at CERN, in: 2012 IEEE Nuclear Science Symposium and Medical Imaging Conference
27 (NSS/MIC), 27 October–3 November 2012, Anaheim, CA, 1199–1203, 2012.
- 28 Guida, R., Carrie, P., De Menezes, L., Duplissy, J., Fayet, F., Haider, S., Kirkby, J., Mathot, S., Minginette, P.,
29 Onnela, A., Rochez, J., Thomas, G., Wasem, A., and Wilhelmsson, M.: Development of the gas system for the
30 CLOUD experiment at CERN, in: Nuclear Science Symposium and Medical Imaging Conference (NSS/MIC),
31 2013 IEEE, Seoul 27 October–2 November 2013, 1–5, 2013.
- 32 Heymsfield, A. J., Miloshevich, L. M., Schmitt, C., Bansemmer, A., Twohy, C., Poellot, M. R., Fridlind, A., and
33 Gerber, H.: Homogeneous Ice Nucleation in Subtropical and Tropical Convection and Its Influence on Cirrus
34 Anvil Microphysics, *J. Atmos. Sci.*, 62, 41-64, doi:10.1175/JAS-3360.1, 2005.
- 35 Heymsfield, A. J., Schmitt, C., Bansemmer, A., and Twohy, C. H.: Improved Representation of Ice Particle
36 Masses Based on Observations in Natural Clouds, *Journal of the Atmospheric Sciences*, 67, 3303-3318,
37 doi:10.1175/2010JAS3507.1, 2010.
- 38 Hirst, E., Kaye, P. H., Greenaway, R. S., Field, P., and Johnson, D. W.: Discrimination of micrometre-sized ice
39 and super-cooled droplets in mixed-phase cloud, *Atmospheric Environment*, 35, 33-47,
40 [http://dx.doi.org/10.1016/S1352-2310\(00\)00377-0](http://dx.doi.org/10.1016/S1352-2310(00)00377-0), 2001.



- 1 Irvine, E. A. and Shine, K. P.: Ice supersaturation and the potential for contrail formation in a changing climate,
- 2 *Earth Syst. Dynam.*, 6, 555-568, doi: 10.5194/esd-6-555-2015, 2015.
- 3 Järvinen, E., Ignatius, K., Nichman, L., Kristensen, T. B., Fuchs, C., Hoyle, C. R., Höppel, N., Corbin, J. C.,
- 4 Craven, J., Duplissy, J., Ehrhart, S., El Haddad, I., Frege, C., Gordon, H., Jokinen, T., Kallinger, P., Kirkby, J.,
- 5 Kiselev, A., Naumann, K.-H., Petäjä, T., Pinterich, T., Prevot, A. S. H., Saathoff, H., Schiebel, T., Sengupta, K.,
- 6 Simon, M., Slowik, J. G., Tröstl, J., Virtanen, A., Vochezer, P., Vogt, S., Wagner, A. C., Wagner, R.,
- 7 Williamson, C., Winkler, P. M., Yan, C., Baltensperger, U., Donahue, N. M., Flagan, R. C., Gallagher, M.,
- 8 Hansel, A., Kulmala, M., Stratmann, F., Worsnop, D. R., Möhler, O., Leisner, T., and Schnaiter, M.:
- 9 Observation of viscosity transition in α -pinene secondary organic aerosol, *Atmos. Chem. Phys.*, 16, 4423-4438,
- 10 doi:10.5194/acp-16-4423-2016, 2016a.
- 11 Järvinen, E., Kemppinen, O., Nousiainen, T., Kociok, T., Möhler, O., Leisner, T., and Schnaiter, M.: Laboratory
- 12 investigations of mineral dust near-backscattering depolarization ratios, *Journal of Quantitative Spectroscopy*
- 13 *and Radiative Transfer*, 178, 192-208, <http://dx.doi.org/10.1016/j.jqsrt.2016.02.003>, 2016b.
- 14 Järvinen, E., M. Schnaiter, G. Mioche, O. Jourdan, V. Shcherbakov, A. Costa, A. Afchine, M. Krämer, F.
- 15 Heidelberg, T. Jurkat, C. Voigt, H. Schlager, L. Nichman, M. Gallagher, E. Hirst, C. Schmitt, A. Bansemmer, A.
- 16 Heymsfield, P. Lawson, U. Tricoli, K. Pfeilsticker, P. Vochezer, O. Möhler, and T. Leisner, 2016: Quasi-
- 17 spherical Ice in Convective Clouds. *J. Atmos. Sci.* doi:10.1175/JAS-D-15-0365.1, in press, 2016c.
- 18 Jeanne, M., Walter, S., and Philip, C.: The Ice Particle Threat to Engines in Flight, in: 44th AIAA Aerospace
- 19 Sciences Meeting and Exhibit, Aerospace Sciences Meetings, American Institute of Aeronautics and
- 20 Astronautics, 2006.
- 21 Jensen, E. J., Lawson, P., Baker, B., Pilon, B., Mo, Q., Heymsfield, A. J., Bansemmer, A., Bui, T. P., McGill, M.,
- 22 Hlavka, D., Heymsfield, G., Platnick, S., Arnold, G. T., and Tanelli, S.: On the importance of small ice crystals
- 23 in tropical anvil cirrus, *Atmos. Chem. Phys.*, 9, 5519-5537, doi: 10.5194/acp-9-5519-2009, 2009.
- 24 Jensen, E., Pfister, L., Bui, T.-P., Lawson, P., and Baumgardner, D.: Ice nucleation and cloud microphysical
- 25 properties in tropical tropopause layer cirrus, *Atmos. Chem. Phys.*, 10, 1369-1384, 2010.
- 26 Johnson, A., Lasher-Trapp, S., Bansemmer, A., Ulanowski, Z., and Heymsfield, A. J.: Difficulties in Early Ice
- 27 Detection with the Small Ice Detector-2 HIAPER (SID-2H) in Maritime Cumuli, *Journal of Atmospheric and*
- 28 *Oceanic Technology*, 31, 1263-1275, doi: 10.1175/JTECH-D-13-00079.1, 2014.
- 29 Johnson, B., Turnbull, K., Brown, P., Burgess, R., Dorsey, J., Baran, A. J., Webster, H., Haywood, J., Cotton,
- 30 R., Ulanowski, Z., Hesse, E., Woolley, A., and Rosenberg, P.: In situ observations of volcanic ash clouds from
- 31 the FAAM aircraft during the eruption of Eyjafjallajökull in 2010, *Journal of Geophysical Research:*
- 32 *Atmospheres*, 117, D00U24, doi: 10.1029/2011JD016760, 2012.
- 33 Kirkby, J., Curtius, J., Almeida, J., Dunne, E., Duplissy, J., Ehrhart, S., Franchin, A., Gagne, S., Ickes, L.,
- 34 Kürten, A., Kupc, A., Metzger, A., Riccobono, F., Rondo, L., Schobesberger, S., Tsagkogeorgas, G., Wimmer,
- 35 D., Amorim, A., Bianchi, F., Breitenlechner, M., David, A., Dommen, J., Downard, A., Ehn, M., Flagan, R. C.,
- 36 Haider, S., Hansel, A., Hauser, D., Jud, W., Junninen, H., Kreissl, F., Kvashin, A., Laaksonen, A., Lehtipalo, K.,
- 37 Lima, J., Lovejoy, E. R., Makhmutov, V., Mathot, S., Mikkilä, J., Minginette, P., Mogo, S., Nieminen, T.,
- 38 Onnela, A., Pereira, P., Petäjä, T., Schnitzhofer, R., Seinfeld, J. H., Sipilä, M., Stozhkov, Y., Stratmann, F.,
- 39 Tomé, A., Vanhanen, J., Viisanen, Y., Vrtala, A., Wagner, P. E., Walther, H., Weingartner, E., Wex, H.,



- 1 Winkler, P. M., Carslaw, K. E., Worsnop, D. R., Baltensperger, U., and Kulmala, M.: Role of sulphuric acid,
2 ammonia and galactic cosmic rays in atmospheric aerosol nucleation, *Nature*, 476, 429–433, 2011.
- 3 Korolev, A., and Isaac, G.: Phase transformation of mixed-phase clouds, *Q. J. R. Meteorol. Soc.*, 129, 19–38,
4 doi: 10.1256/qj.01.203, 2003a.
- 5 Korolev, A., and Isaac, G.: Roundness and Aspect Ratio of Particles in Ice Clouds, *J. Atmos. Sci.*, 60, 1795–
6 1808, doi: 10.1175/1520-0469(2003)060<1795:RAAROP>2.0.CO;2, 2003b.
- 7 Korolev, A. V., Isaac, G. A., Cober, S. G., Strapp, J. W., and Hallett, J.: Microphysical characterization of
8 mixed-phase clouds, *Q. J. R. Meteorol. Soc.*, 129, 39–65, 10.1256/qj.01.204, 2003c.
- 9 Lawson, R. P., Heymsfield, A. J., Aulenbach, S. M., and Jensen, T. L.: Shapes, sizes and light scattering
10 properties of ice crystals in cirrus and a persistent contrail during SUCCESS, *Geophysical Research Letters*, 25,
11 1331–1334, doi: 10.1029/98GL00241, 1998.
- 12 Lawson, R. P. B., Baker, B. A., and Pilson, B. A.: In-situ measurements of microphysical properties of mid-
13 latitude and anvil cirrus, in: *Proceedings, 30th International Symposium on Remote Sensing Environment*,
14 Honolulu, Hawaii, 10–14 November, 707–710, 2003.
- 15 Lawson, R. P., Baker, B., Pilson, B., and Mo, Q.: In Situ Observations of the Microphysical Properties of Wave,
16 Cirrus, and Anvil Clouds. Part II: Cirrus Clouds, *J. Atmos. Sci.*, 63, 3186–3203, doi:10.1175/JAS3803.1, 2006.
- 17 Luebke, A. E., Afchine, A., Costa, A., Meyer, J., Rolf, C., Spelten, N., Avallone, L. M., Baumgardner, D., and
18 Krämer, M.: The origin of midlatitude ice clouds and the resulting influence on their microphysical properties,
19 *Atmos. Chem. Phys. Discuss.*, 15, 34243–34281, doi: 10.5194/acpd-15-34243-2015, 2015.
- 20 Lynch, D. K.: *Cirrus*, Oxford University Press, 2001.
- 21 Möhler, O., Field, P. R., Connolly, P., Benz, S., Saathoff, H., Schnaiter, M., Wagner, R., Cotton, R., Krämer,
22 M., Mangold, A., and Heymsfield, A. J.: Efficiency of the deposition mode ice nucleation on mineral dust
23 particles, *Atmos. Chem. Phys.*, 6, 3007–3021, doi:10.5194/acp-6-3007-2006, 2006.
- 24 Nelson, J.: Sublimation of Ice Crystals. *J. Atmos. Sci.* 55, 910–919 (1998).
- 25 Nichman, L., Fuchs, C., Järvinen, E., Ignatius, K., Höppel, N. F., Dias, A., Heinritzi, M., Simon, M., Tröstl, J.,
26 Wagner, A. C., Wagner, R., Williamson, C., Yan, C., Connolly, P. J., Dorsey, J. R., Duplissy, J., Ehrhart, S.,
27 Frege, C., Gordon, H., Hoyle, C. R., Kristensen, T. B., Steiner, G., McPherson Donahue, N., Flagan, R.,
28 Gallagher, M. W., Kirkby, J., Möhler, O., Saathoff, H., Schnaiter, M., Stratmann, F., and Tomé, A.: Phase
29 transition observations and discrimination of small cloud particles by light polarization in expansion chamber
30 experiments, *Atmos. Chem. Phys.*, 16, 3651–3664, doi:10.5194/acp-16-3651-2016, 2016.
- 31 Petzold, A., Esselborn, M., Weinzierl, B., Ehret, G., Ansmann, A., Müller, D., Donovan, D., van Zadelhoff, G.-
32 J., Berthier, S., Wiegner, M., Gasteiger, J., Buras, R., Mayer, B., Lajas, D., and Wehr, T.: ICAROHS inter-
33 comparison of aerosol retrievals and observational requirements for multi-wavelength HSRL systems, in:
34 *Proceedings of the ESA Living Planet Symposium*, Bergen, Norway, ESA SP-686, December 2010, edited by:
35 Lacoste-Francis, H., ESA Communications published and distributed by: ESA Communications, ESTEC,
36 Noordwijk, the Netherlands, p. 102, 2010.
- 37 Rosenfeld, D., and Woodley, W. L.: Deep convective clouds with sustained supercooled liquid water down to -
38 37.5 °C, *Nature*, 405, 440–442, 2000.



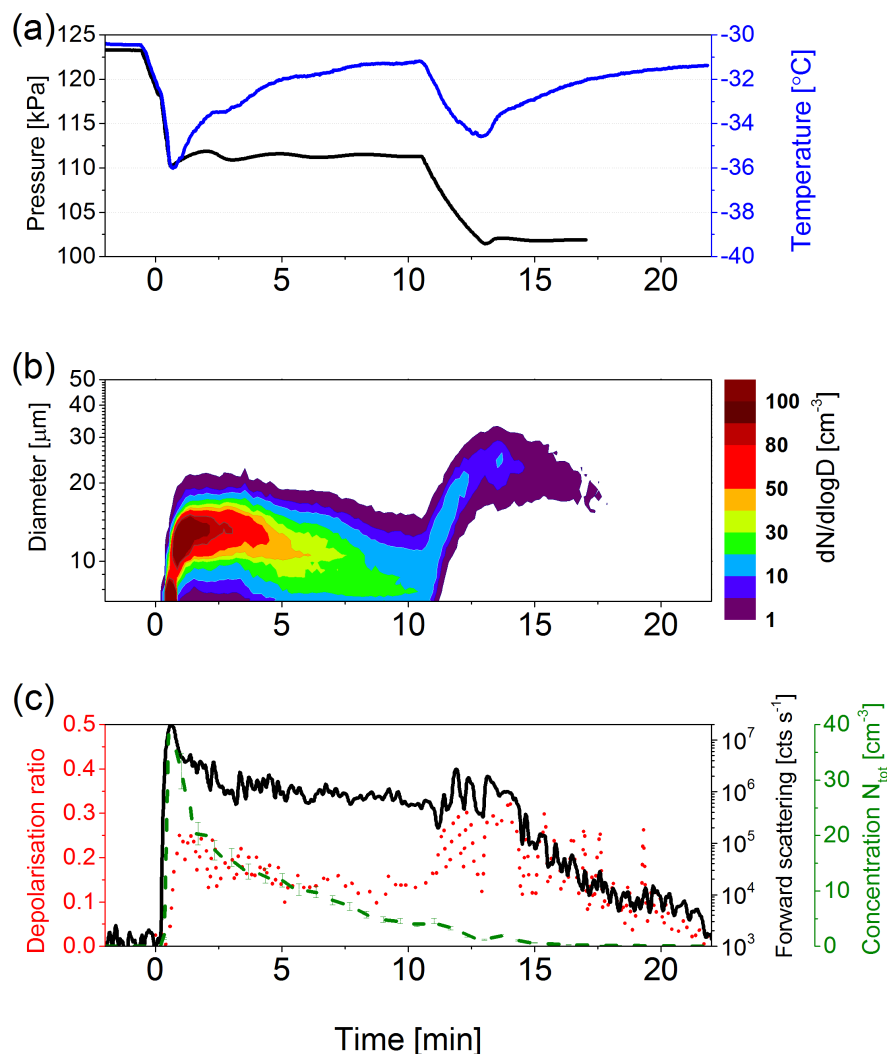
- 1 Sachweh, B., Barthel, H., Polke, R., Umhauer, H., and Büttner, H.: Particle shape and structure analysis from
2 the spatial intensity pattern of scattered light using different measuring devices, *J. Aerosol Sci.*, 30, 1257-1270,
3 [http://dx.doi.org/10.1016/S0021-8502\(99\)00045-2](http://dx.doi.org/10.1016/S0021-8502(99)00045-2), 1999.
- 4 Schnaiter, M., Büttner, S., Möhler, O., Skrotzki, J., Vragel, M., and Wagner, R.: Influence of particle size and
5 shape on the backscattering linear depolarisation ratio of small ice crystals – cloud chamber measurements in
6 the context of contrail and cirrus microphysics, *Atmos. Chem. Phys.*, 12, 10465–10484, doi:10.5194/acp-12-
7 10465-2012, 2012.
- 8 Schnaiter, M., Järvinen, E., Vochezer, P., Abdelmonem, A., Wagner, R., Jourdan, O., Mioche, G., Shcherbakov,
9 V. N., Schmitt, C. G., Tricoli, U., Ulanowski, Z., and Heymsfield, A. J.: Cloud chamber experiments on the
10 origin of ice crystal complexity in cirrus clouds, *Atmos. Chem. Phys.*, 16, 5091-5110, doi:10.5194/acp-16-5091-
11 2016, 2016.
- 12 Stith, J. L., Avallone, L. M., Bansemer, A., Basarab, B., Dorsi, S. W., Fuchs, B., Lawson, R. P., Rogers, D. C.,
13 Rutledge, S., and Toohey, D. W.: Ice particles in the upper anvil regions of midlatitude continental
14 thunderstorms: the case for frozen-drop aggregates, *Atmos. Chem. Phys.*, 14, 1973-1985, doi:10.5194/acp-14-
15 1973-2014, 2014.
- 16 Stordal, F., Myhre, G., Stordal, E. J. G., Rossow, W. B., Lee, D. S., Arlander, D. W., and Svendby, T.: Is there a
17 trend in cirrus cloud cover due to aircraft traffic?, *Atmos. Chem. Phys.*, 5, 2155-2162, doi:10.5194/acp-5-2155-
18 2005, 2005.
- 19 Taylor, J. W., Choulaton, T. W., Blyth, A. M., Liu, Z., Bower, K. N., Crosier, J., Gallagher, M. W., Williams,
20 P. I., Dorsey, J. R., Flynn, M. J., Bennett, L. J., Huang, Y., French, J., Korolev, A., and Brown, P. R. A.:
21 Observations of cloud microphysics and ice formation during COPE, *Atmos. Chem. Phys.*, 16, 799-826,
22 doi:10.5194/acp-16-799-2016, 2016.
- 23 Vochezer, P., Järvinen, E., Wagner, R., Kupiszewski, P., Leisner, T., and Schnaiter, M.: In situ characterization
24 of mixed phase clouds using the Small Ice Detector and the Particle Phase Discriminator, *Atmos. Meas. Tech.*,
25 9, 159-177, doi: 10.5194/amt-9-159-2016, 2016.
- 26 Wagner, R., Benz, S., Bunz, H., Möhler, O., Saathoff, H., Schnaiter, M., Leisner, T., and Ebert, V.: Infrared
27 optical constants of highly diluted sulfuric acid solution droplets at cirrus temperatures, *J. Phys. Chem. A*, 112,
28 11661–11676, 2008.
- 29 Wendisch, M., and Brenguier, J.-L.: *Airborne Measurements for Environmental Research: Methods and*
30 *Instruments*, John Wiley & Sons, 2013.
- 31 Zhang, C., and Harrington, J. Y.: The Effects of Surface Kinetics on Crystal Growth and Homogeneous
32 Freezing in Parcel Simulations of Cirrus, *J. Atmos. Sci.*, 72, 2929-2946, doi: 10.1175/JAS-D-14-0285.1, 2015.
- 33



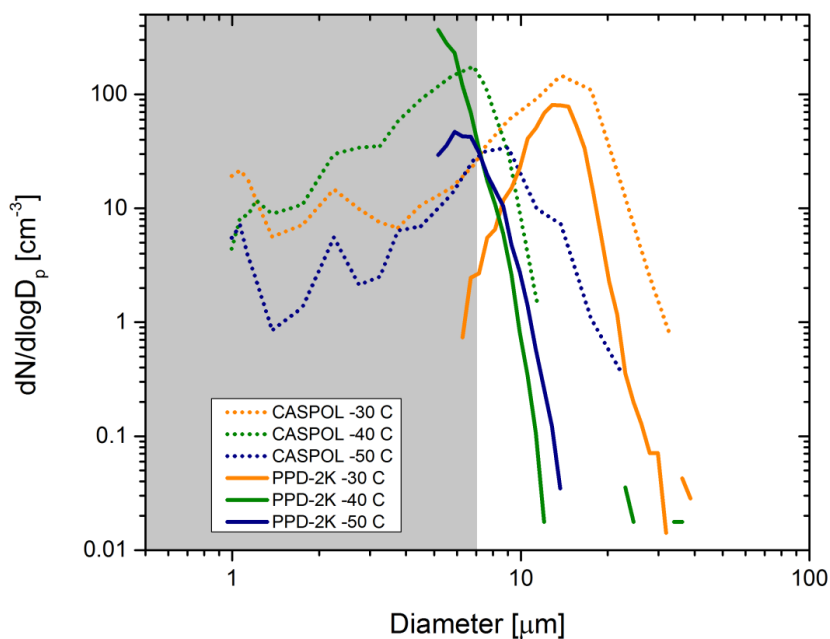
1 **Table 1: List of experiments**

Exp. number	CCN conc. [cm ⁻³]	Cooling rate [°C min ⁻¹]	T start [°C]	Mean diameter [μm]	Mean dN/dlogD _p [cm ⁻³]
1276.05	220	-5	-40	7.9	48
1291.07	160	-5.8	-30	10	41.7
1291.12	110	-4.8	-30	15	30
1292.01	150	-4.9	-30	12	41.7
1298.12	110	-2.1	-50	9	6.5
1298.20	750	-3.1	-50	8	9.9

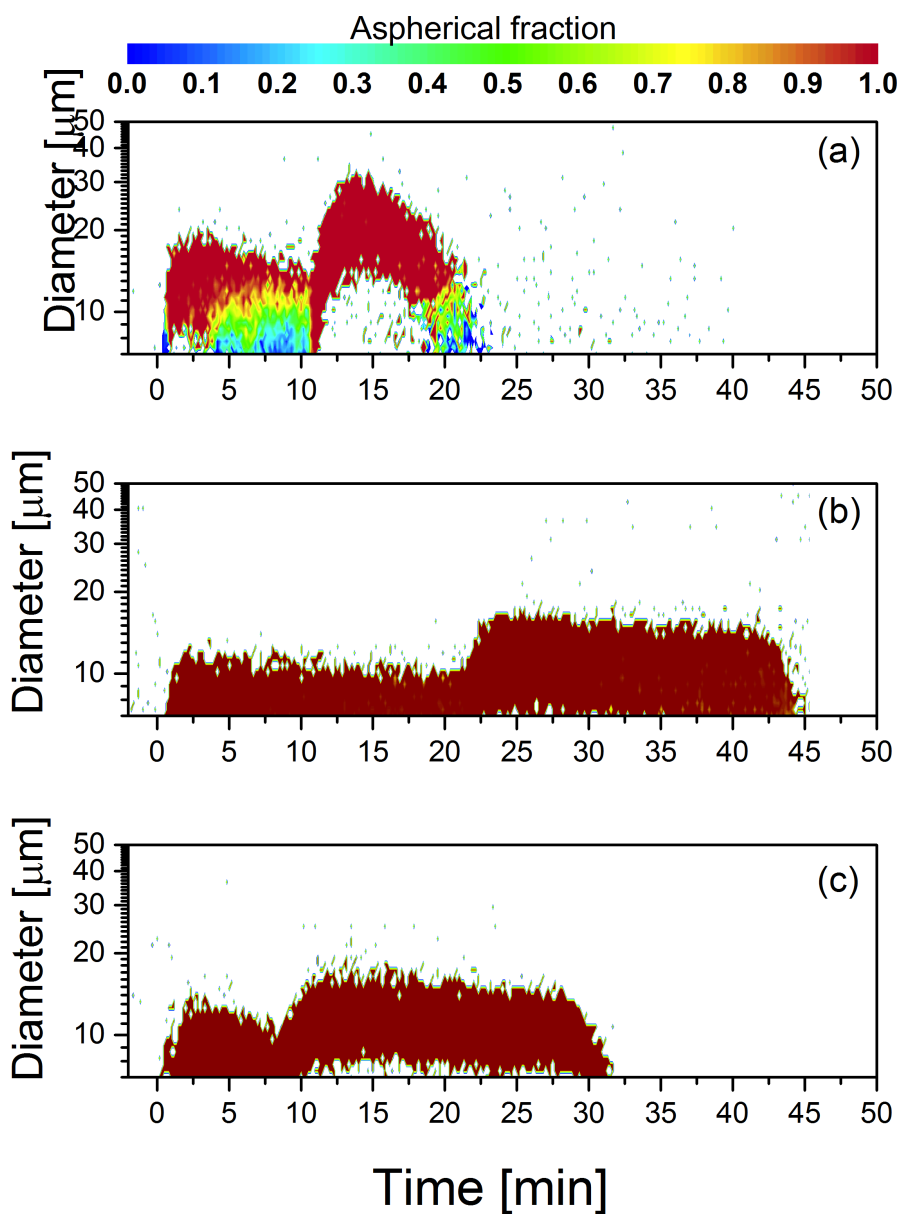
2



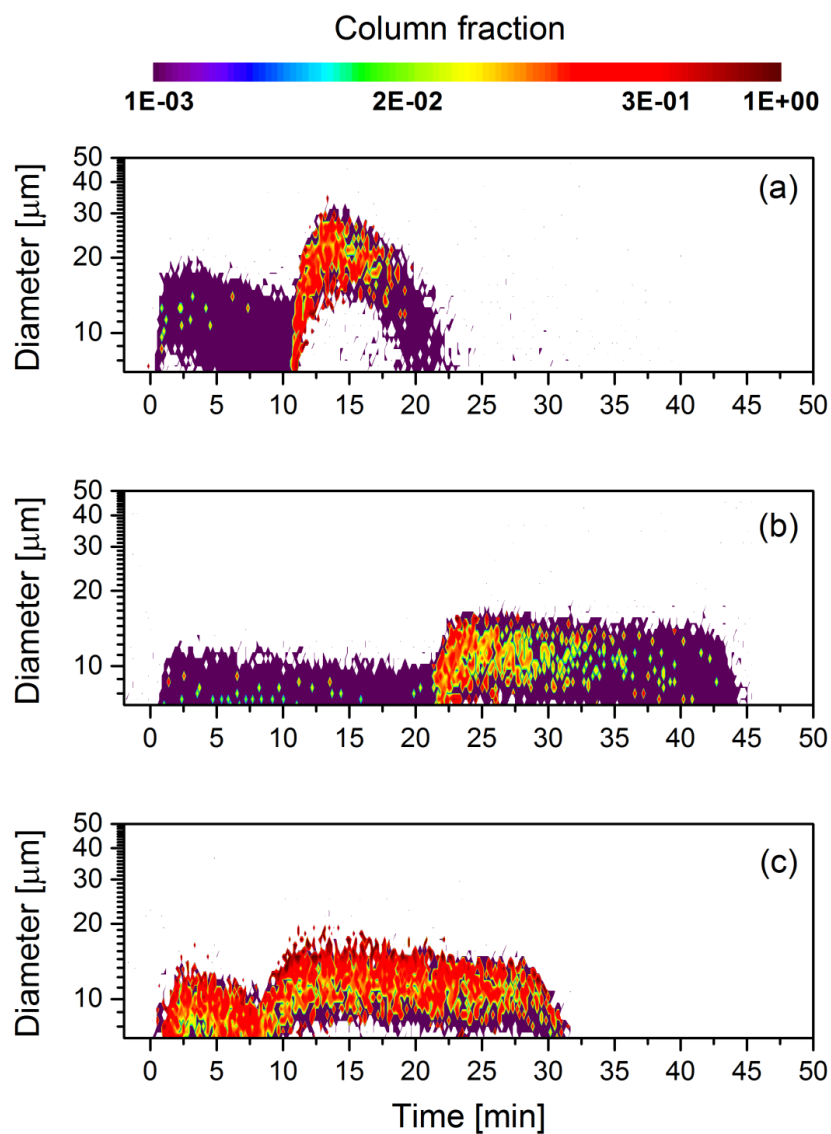
1
2 **Figure 1. Homogeneous ice nucleation and regrowth experiment no. 1292.01 (-30 °C).** (a) The development of
3 pressure and temperature. Cloud forms at $t=0$ min, (b) The size distribution measured with PPD-2K, (c) SIMONE
4 measurements of the forward scattering intensity (black solid line) and depolarisation ratio (red dotted line) together
5 with the total number concentration measured by the PPD-2K (green dashed line).



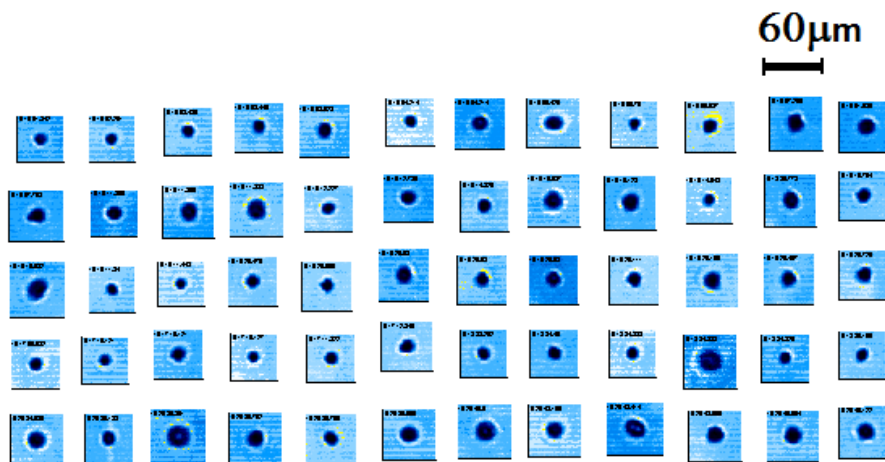
1
2 **Figure 2.** Selected 1 min averaged particle size distributions for runs: 1292.01 (–30 °C), 1276.05 (–40 °C), 1298.12 (–50
3 °C). White area represents the overlap in the size range of PPD-2K and CASPOL. Grey area represents the particles
4 that are mostly present in the 292 PBP polarisation data points in a second. The aspherical fraction for comparison in
5 Fig. 6 is derived from the white area.



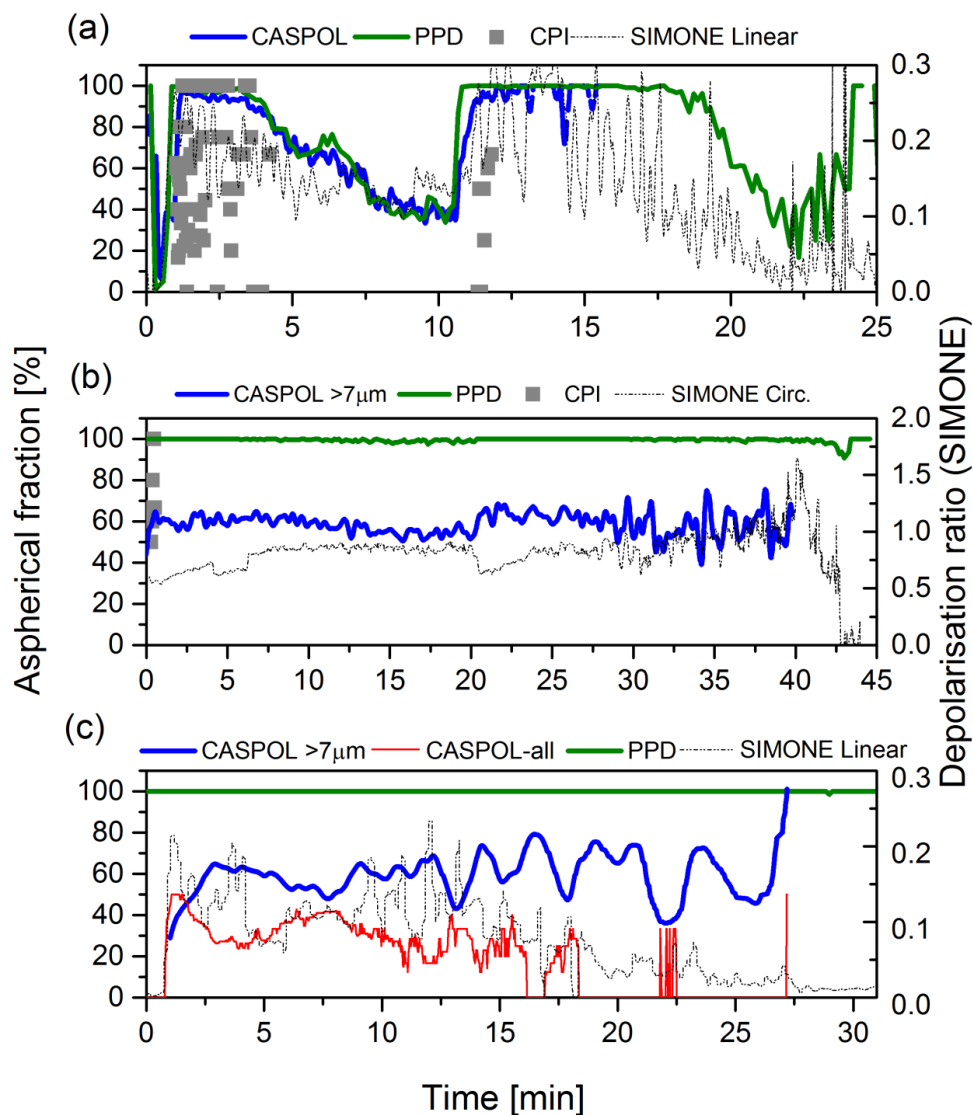
1
2 **Figure 3.** Size-segregated aspherical fraction measured by PPD-2K (see Sect. 2.3.1). (a) Run no. 1292.01 ($-30\text{ }^{\circ}\text{C}$), (b)
3 Run no. 1276.05 ($-40\text{ }^{\circ}\text{C}$), (c) Run no. 1298.12 ($-50\text{ }^{\circ}\text{C}$).



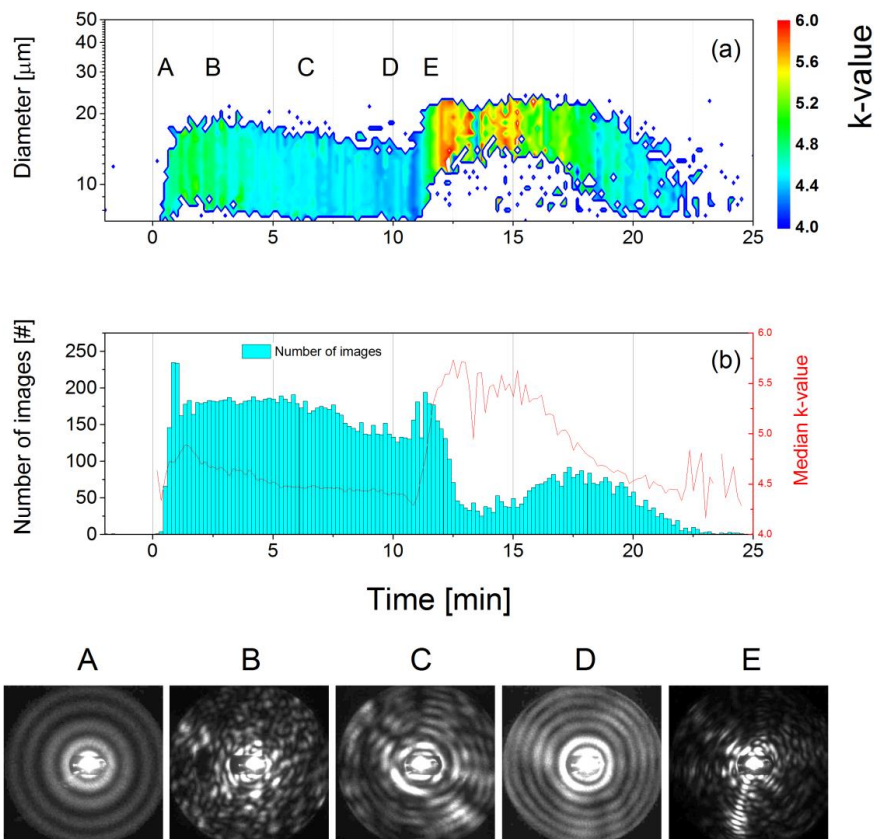
1
2 Figure 4. Size segregated fraction of columns on log scale, measured by PPD-2K. (a) Run no. 1292.01 ($-30\text{ }^\circ\text{C}$), (b)
3 Run no. 1276.05 ($-40\text{ }^\circ\text{C}$), (c) Run no. 1298.12 ($-50\text{ }^\circ\text{C}$).



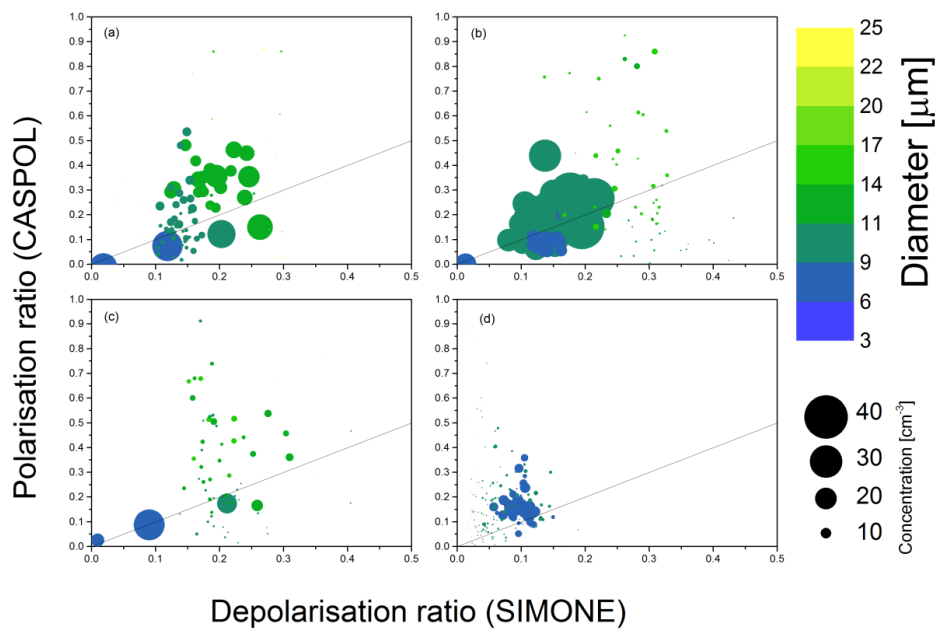
1
2 Figure 5. Experiment no. 1292.01. 3V-CPI images of frozen droplets immediately after phase transition. Shape
3 analysis of these particles is presented in Fig.6.



1
 2 **Figure 6.** PPD-2K (green line), CASPOL (blue line) aspherical fraction of a subgroup of particles with diameter > 7
 3 μm . The inter-comparison complemented by SIMONE linear or circular depolarisation ratio (dashed line), CASPOL
 4 aspherical fraction for all diameters (red line) and 3V- CPI non-round (aspherical) fraction (grey rectangles). (a) Run
 5 no. 1292.01 (-30°C), (b) Run no. 1276.05 (-40°C), (c) Run no. 1298.12 (-50°C).



1
2 **Figure 7.** Evolution of small-scale complexity in experiment 1292.01 ($-30\text{ }^{\circ}\text{C}$). (a) The size-segregated k-value
3 (complexity parameter), capital letters correspond to the scattering patterns presented at the bottom, (b) Number of
4 the scattering images used for the analysis and the median k-value. Lowest panel: 2-D scattering patterns from PPD-
5 2K that have been collected during periods indicated with the letters A–E. For size segregated k-values at lower
6 temperatures see Fig. S2.



1
2 **Figure 8.** CASPOL polarisation and SIMONE depolarisation comparison for runs (a) no. 1292.01, (b) no. 1291.07, (c)
3 no. 1291.12, (d) no. 1298.20, for details see Table 1. Marker size annotates number concentration, with highest at 56
4 cm^{-3} . Diameter is colour coded. Black reference line is 1:1 ratio.